



Published in final edited form as:

*Conf Proc IEEE Eng Med Biol Soc.* 2019 July ; 2019: 2765–2768. doi:10.1109/EMBC.2019.8857103.

## A Pipeline for the Registration of Calcium Transient Data to Structural Networks of the Interstitial Cells of Cajal.

Anna Qian<sup>1</sup>, Shawn Means<sup>1</sup>, John Malysz<sup>3</sup> [Assistant Professor Pharmaceutical Sciences], Gianrico Farrugia<sup>2</sup>, Simon J. Gibbons<sup>2</sup>, Peng Du<sup>1</sup>

<sup>1</sup>Auckland Bioengineering Institute, University of Auckland, New Zealand <sup>2</sup>Enteric NeuroScience Program, Mayo Clinic, Rochester, MN, USA <sup>3</sup>University of Tennessee Health Science Center, 575 COLLEGE OF PHARMACY BUILDING, 881 MADISON AVENUE, MEMPHIS TN 38163

### Abstract

Interstitial cells of Cajal (ICC) generate electrical pacemaker activity in the gastrointestinal (GI) tract known as slow waves, which regulate GI motility. ICC express both the Kit receptor tyrosine kinase protein and a  $Ca^{2+}$ -activated  $Cl^-$ -channel, encoded by the anoctamin1 (Ano1) protein, which is an essential contributor to the  $Ca^{2+}$  cycling of ICC and slow wave pacemaking. Recent dye-loading imaging studies have demonstrated  $Ca^{2+}$  transients in ICC in isolated tissue preparations. The main aim of this study was to develop a method that allows  $Ca^{2+}$  transients to be registered to structural ICC network data. Confocal image stacks of ICC labeled for Kit or Ano1 and  $Ca^{2+}$  recording data were processed using a thresholding protocol. The  $Ca^{2+}$  transients were then registered to the ICC structural network. First, a general idea of the placement was found by mapping the field-of-view of the  $Ca^{2+}$  transient data to the distorted tissue that contained the ICC network image. The errors in the registration were then corrected for by warping the internal  $Ca^{2+}$  transient field according to the structural network. In data sets from tissues with induced, targeted knockdown of Ano1 expression in a subset of ICC, agreement between the  $Ca^{2+}$  transient data and structural network was  $68 \pm 10\%$ . This level of agreement allowed selective extraction of  $Ca^{2+}$  data from Ano1-positive (Ano1+) and Ano1-negative (Ano1-) ICC. In the future, this technique will allow investigation into the functional properties of ICC in relation to the level of knockdown of specific ICC associated proteins.

### I. Introduction

Contractions in the gastrointestinal (GI) tract are in part governed by electrophysiological events called slow waves [1]. Slow waves are generated spontaneously by, and propagated through a dense network of pacemaker cells called the interstitial cells of Cajal (ICC), which are distributed throughout the GI tract. ICC form close coupling with GI smooth muscle cells and coordinate excitation-contraction coupling mechanisms in the GI tract [2].

The generation of slow wave activity is driven by an intrinsic cycling of  $Ca^{2+}$  in the ICC, through the cyclical and measurable transients of the cytosolic  $Ca^{2+}$  concentration.  $Ca^{2+}$  is

released from inositol 1,4,5-triphosphate (IP3)-mediated channels in the endoplasmic reticulum (ER) into the cytosol. The depletion of the ER triggers  $\text{Ca}^{2+}$  influx from extracellular space. The cytosolic increase in  $[\text{Ca}^{2+}]_i$  activates  $\text{Ca}^{2+}$ -dependent ion channels, leading to the depolarization of ICC and slow wave activity [1,3].

The  $\text{Ca}^{2+}$ -activated  $\text{Cl}^-$ -channel encoded by Anoctamin1 (Ano1, aka TMEM16A) plays a critical role in the generation and regulation of slow waves in the GI tract [4,5]. Ano1 is a reliable marker of ICC as it identifies all ICC labeled by the traditionally used Kit marker [6].

The development of a genetically modified mouse strain with targeted, conditional knockout (KO) of Ano1 expression has allowed for the investigation of the effects of Ano1 KO in adult mice ICC in terms of slow waves, motility and  $\text{Ca}^{2+}$  transients [5,7]. These investigations have largely been based on excised tissues that contained a mixture of Ano1+ and Ano1- cells in close proximity to each other. Observations show abnormal transients occurring in preparations with a high proportion of Ano1- ICC [7]. However, the interactions between the  $\text{Ca}^{2+}$  transients from Ano1+ and Ano1- ICC remain incompletely understood.

The main aim of this study was to develop a method to register  $\text{Ca}^{2+}$  activities and ICC networks labeled for Ano1+ and Ano1- regions of the Kit-positive ICC network in the field-of-view (FOV). The combined data can be used to investigate the impact of Ano1 loss at a micro-scale.

## II. Method

### A. Tissue Preparation and Imaging

Data from six transgenic mice, treated with tamoxifen to induce recombination and partial knockout of Ano1 expression, were obtained using previously established protocols [7]. Cal520AM dye was used to measure  $\text{Ca}^{2+}$  transients in the ICC-MY network. The FOV of the  $\text{Ca}^{2+}$  transient studies was marked by a UV laser at the end of the experiment. Data was recorded at 4.5 frames-per-second across 66 seconds (300 frames), saved as 16-bit .tiff files, and processed in ImageJ. Following  $\text{Ca}^{2+}$  imaging studies, the tissues were prepared for immunohistochemical staining for the total ICC network (Kit) and Ano1 protein expression and images were collected from the tagged FOV using a laser scanning confocal microscope (Olympus, Center Valley, PA, USA) with a 20X 0.95 NA objective, as previously described [7]. The resolution in the optical axis was  $1.13 \mu\text{m}$  and the number of optical sections for each sample was dependent on the tissue thickness, varying between 26 and 48 slices per sample.

### B. ICC network extraction from Kit/Ano1 images

The six datasets were processed in MATLAB (version 2018b, The MathWorks, Inc., Natick, MA, USA) using the following protocol:

1. All frames of the Kit and Ano1 images were summed linearly in the z-axis/transmural direction.

2. The resultant image was linearly interpolated in the  $(x, y)$  direction, such that each pixel represents  $1 \mu m$ .
3. A thresholding was performed on the resultant image to find a mask of the ICC network identified by the immunohistochemical markers. The thresholding was performed using Otsu's method [8], which assumes a bimodal histogram in the intensity of pixels and minimises variance between classes of pixels, i.e., those that were labeled by the markers and those that were not. If the outcome of a binary threshold was not sufficiently selective, the thresholding was repeated, separating the image into three intensity layers, and selecting the layer with the highest intensity as the mask.

The resultant Kit and Ano1 labeled ICC networks were overlaid to identify structures within the FOV that were Ano1 positive (Kit+/Ano1+) or Ano1 negative (Kit+/Ano1-). The error was calculated using the following equation as the ratio between Ano1+ regions that did not overlap with Kit regions (Ano1+/Kit-) and Ano1+ regions that overlapped with Kit regions (Ano1+/Kit+),

$$Error = \frac{Ano1+ / Kit-}{Ano1+ / Kit+} \quad (1)$$

### C. Data extraction from Ca<sup>2+</sup> Imaging Data

We analyzed Ca<sup>2+</sup> transient data using ImageJ (version 1.51n, NIH, USA) plug-ins and custom MATLAB routines [7]. Frames were corrected for movement artifacts using the WalkingAverage plugin in ImageJ [9]. The following protocol was used to extract the locations of active Ca<sup>2+</sup> regions from the Ca<sup>2+</sup> transient data.

1. Identify regions of activity using background subtraction. The background model was created using frame difference (Eq. 2) [10],

$$B_i = \frac{1}{L} \sum_{t=1}^{i+L} Z_t \quad (2)$$

$$R_i(x, y) = \begin{cases} \left| \frac{Z_j - B_i}{B_i} \right|, & \text{if } \left| \frac{Z_j - B_i}{B_i} \right| > T \\ 0, & \text{otherwise} \end{cases} \quad (3)$$

where  $B$  is the background at time  $i$ ,  $Z$  refers to the video frames,  $L$  is the number of frames to average ( $L = 5$ ) and  $t \in \{0, z - L\}$ . The relative difference between the background model and the frame of interest was found. A threshold was also applied (Eq. 3), where  $T$  is the threshold ( $T = 0.3$ ) and  $j = i + L + 1$  to reduce noise.

2. Sum all resultant frames linearly in the z-axis/temporally.

3. The summed image was linearly interpolated in the  $(x, y)$  direction, such that each pixel represents the same resolution as the immunohistochemical images. This also has a gaussian smoothing effect on the resultant image.
4. Apply contrast stretching to the image to enhance the contrast between regions of  $\text{Ca}^{2+}$  transient and the background, by using the *imadjust* and *stretchlim* functions in MATLAB.
5. A thresholding was performed in the same way as for the immunohistochemical images to create a mask that identifies the location of  $\text{Ca}^{2+}$  activity. The mask was applied over the result of *Step 4* in order to preserve information on the intensity of the  $\text{Ca}^{2+}$  activity.

#### D. Network Registration and Validation

The  $\text{Ca}^{2+}$  transients were assumed to originate from the ICC-MY networks so that the  $\text{Ca}^{2+}$  transient data could be registered to the immunohistochemical data. A network registration process was undertaken to align these two datasets to account for the differences in zoom and position when imaging the two datasets, and the structural deformation in the tissue as a result of the imaging preparation process. The registration process consisted of two stages:

1. With consideration of the  $\text{Ca}^{2+}$  FOV, a general level of deformation in the tissue was estimated. Eight points were marked manually along the boundary of the FOV (Fig. 1b). A transformation matrix was calculated, and was then applied to each frame of the  $\text{Ca}^{2+}$  imaging data using MATLAB functions *fitgeotrans* and *imwarp*. The same transformation matrix was applied to the thresholded  $\text{Ca}^{2+}$  transient data from Part C.

A gelatin phantom was created to test the accuracy of the registration process with consideration of deformation in the boundary only (Fig. 2). A square grid was labeled across an area in the centre of a thin layer of gelatin (Fig. 2a). An image of the undeformed phantom was taken at close range to represent the  $\text{Ca}^{2+}$  recording. The phantom was deformed and an image was taken from a larger distance to represent the immunohistochemical stained images. Using the eight boundary points on both the deformed and undeformed gelatin, we were able to mimic the deformation using the transformation process with an average error of 0.5% across all marked grid points (Fig. 2b).

2. Internal deformation cannot be accounted for by consideration of the external boundary points only. The extracted  $\text{Ca}^{2+}$  transient data and structural networks were aligned in Adobe Photoshop CC 2018 (version 19.0, Adobe Inc., San Jose, CA, USA) using the *puppet warp* function. Care was taken to minimize the shift the boundary of the  $\text{Ca}^{2+}$  transient data in order to preserve the  $\text{Ca}^{2+}$  FOV.

The accuracy of the registration process was calculated quantitatively by measuring the proportion of overlap between the regions exhibiting  $\text{Ca}^{2+}$  transients and the structural network, using the following equation,

$$Error = \frac{Ca^{2+} + / ICC +}{Ca^{2+} +} \quad (4)$$

### III. Results and Discussion

The network thresholding protocol was able to extract the structural distribution of ICC. Fig. 3a presents an overlay of the post-threshold Kit and Ano1 labeled tissue images. Given Kit and Ano1 equally identify ICC-MY [6], the average error in agreement between Kit and Ano1 identified structures was  $6 \pm 1.56\%$ . Across samples, the density of ICC was  $28 \pm 4.7\%$  and of all ICC, the average percentage of Ano1+ ICC was  $18 \pm 5\%$ .

The  $Ca^{2+}$  recording data was processed to identify regions that exhibit  $Ca^{2+}$  transients where regions with more  $Ca^{2+}$  transients were presented brighter than regions with less  $Ca^{2+}$  transients. Intense activity appear scattered in small localised regions across the FOV. These high intensity regions are connected by thin spindle-shaped regions with lower intensity transients, as shown in (Fig. 3b)

Registration of  $Ca^{2+}$  transient data to the ICC network was performed in two stages. Following registration of the  $Ca^{2+}$  activity to the  $Ca^{2+}$  imaging FOV, distinct structural similarities can be seen between the ICC network and the location of the  $Ca^{2+}$  transients (Fig. 4a). In most cases, the origin of  $Ca^{2+}$  activity can be attributed directly to ICC, demonstrated by the general good alignment between the two sets of data. The features formed an adequate guide for the spatial warping process of the  $Ca^{2+}$  transient data which resulted in an improvement to the overlap between  $Ca^{2+}$  transients and ICC, particularly to regions of high intensity activity (Fig. 4b). The average accuracy in the registration was  $49 \pm 8.6\%$  prior to warping (Fig. 4a) of  $Ca^{2+}$  transients and increases to  $68 \pm 10\%$  post-warping (Fig. 4b).

The average proportion of Ano1+ regions was  $19 \pm 5\%$  across the entire immunohistochemical image FOV and  $20 \pm 10\%$  across the  $Ca^{2+}$  imaging FOV, which indicates that the  $Ca^{2+}$  activity within the FOV was a fair representation of the tissue as a whole.

The registered images provided a guide the correlation between Ano1– regions and  $Ca^{2+}$  transients.  $Ca^{2+}$  transients from a selection of Ano1+/Kit+ and Ano1–/Kit+ ICC were extracted (Fig. 5). In general, the  $Ca^{2+}$  transients extracted from Ano1+ regions in the FOV demonstrated regular activities (Fig. 5a). On the other hand, the  $Ca^{2+}$  transients extracted from the Ano1– regions contained a combination of regular activity that was identical to the Ano1+ region activity, and activities that demonstrated significant reduction in frequency and/or irregularity in the rhythm (Fig. 5b)..

While the deformation of the gelatin phantom produced a good agreement between the deformed phantom and warped data, the deformations of the real tissue during the staining process were much more complex. Additional factors such as incomplete staining, background signal from non-specific labeling, and uneven tissue surface all impacted on the

accuracy of the registration between the  $\text{Ca}^{2+}$  transient data and labeled ICC network. Another potential source of error was the manual placements of the boundary points of  $\text{Ca}^{2+}$  transient FOV in the deformed tissue after staining. Given deformation was likely non-linear, errors could be introduced from the deformation matrix. In future, more sophisticated soft tissue deformation techniques should be applied to better account for the tissue deformation during the staining process. Nevertheless, the proposed pipeline demonstrated the usefulness of investigating  $\text{Ca}^{2+}$  transient in relation to the spatial locations of cells and labeled channels.

#### IV. Conclusion

A pipeline for the registration of dye-loading  $\text{Ca}^{2+}$  transient data to immunohistochemical stained ICC networks and Ano1 channels was developed. The technique was validated in a gelatin phantom and then applied in data obtained from mouse small intestinal tissue. We were able to register  $\text{Ca}^{2+}$  activity recorded over the same region to this structural network. This will allow further investigation into the direct impact of loss of Ano1 or other ICC-associated proteins on ICC function as measured using fluorescent reporters of ion concentrations and membrane voltage.

#### Acknowledgments

This work was supported in part by the Rutherford Foundation administered by the Royal Society of New Zealand and by NIH R01 DK57061.

#### References

- [1]. Huizinga J and Lammers W, "Gut peristalsis is governed by a multitude of cooperating mechanisms." *A J Physiol*, vol. 296, no. 1, pp. G1–8, 2009.
- [2]. Sanders K, Koh S et al., "Regulation of gastrointestinal motility - insights from smooth muscle biology." *Nat Rev Gastroenterol Hepatol*, vol. 9, no. 11, pp. 633–645, 2012. [PubMed: 22965426]
- [3]. Nakayama S, Kajioka S et al., "Calcium-associated mechanisms in gut pacemaker activity." *J Cell Mol Med*, vol. 11, no. 5, pp. 958–968, 2007. [PubMed: 17979877]
- [4]. Singh R, Gibbons S et al., "Ano1, a  $\text{Ca}^{2+}$ -activated  $\text{Cl}^-$  channel, coordinates contractility in mouse intestine by  $\text{Ca}^{2+}$  transient coordination between interstitial cells of cajal." *J Physiol*, vol. 592, no. 18, pp. 4051–68, 2014. [PubMed: 25063822]
- [5]. Hwang S, Blair P et al., "Expression of anoctamin 1/*tmem16a* by interstitial cells of cajal is fundamental for slow wave activity in gastrointestinal muscles." *J Physiol*, vol. 587, no. 20, pp. 4887–4904, 2009. [PubMed: 19687122]
- [6]. Gomez-Pinilla P, Gibbons S et al., "Ano1 is a selective marker of interstitial cells of cajal in the human and mouse gastrointestinal tract." *Am J Physiol Gastrointest Liver Physiol*, vol. 296, no. 6, pp. G1370–G1381, 2009. [PubMed: 19372102]
- [7]. Malysz J, Gibbons S et al., "Conditional genetic deletion of *ano1* in interstitial cells of cajal impairs  $\text{Ca}^{2+}$  transients and slow-waves in adult mouse small intestine." *Am J Physiol Gastrointest Liver Physiol*, 2016.
- [8]. Otsu N, "A threshold selection method from gray-level histograms." *IEEE Transactions on Systems, Man, and Cybernetics*, vol. 9, no. 1, pp. 62–66, 1979.
- [9]. Rietdorf J and Seitz A. (2008) Kymograph (time space plot) plugin for imagej. [Online]. Available: "[https://www.embl.de/eamnet/html/body\\_kymograph.html](https://www.embl.de/eamnet/html/body_kymograph.html)"
- [10]. Sobral A and Vacavant A, "A comprehensive review of background subtraction algorithms evaluated with synthetic and real videos." *Comput Vis Image Underst*, vol. 122, pp. 4–21, 2014.

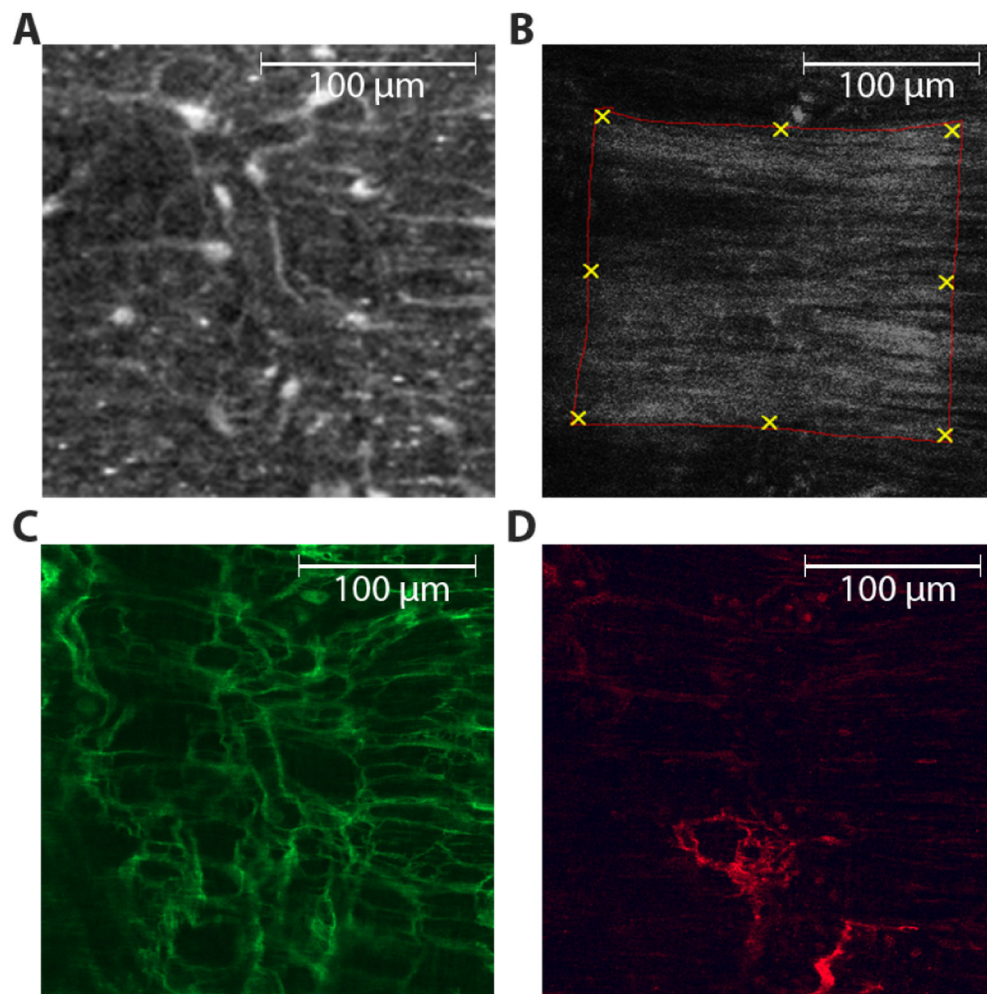


**Fig. 1:** Tissue preparation and imaging: (a) Sample frame of Ca<sup>2+</sup> recording. (b) Ca<sup>2+</sup> recording FOV marked within immunohistochemical imaging FOV, which is highlighted in the red box. Corner and boundary points were manually selected (yellow crosses). Sample frame of (c) Kit and (d) Anol positive ICC in the FOV.

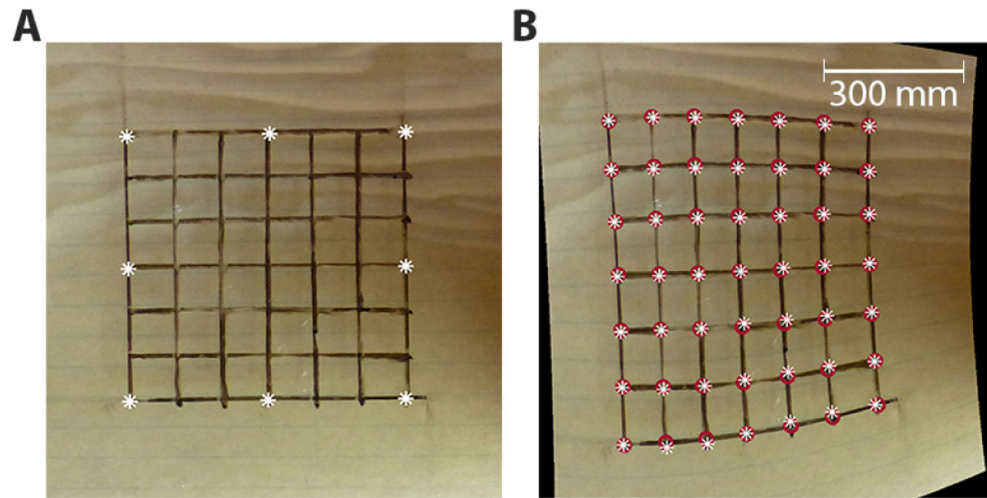


**Fig. 2:**  
A demonstration of registration with consideration of boundary deformation only. (a) Undeformed phantom with boundary points labeled as white asterisks. (b) Computationally transformed phantom. Red circle markers indicate the locations of grid points on the computationally transformed model and white asterisks indicate the actual corresponding location on the deformed phantom.

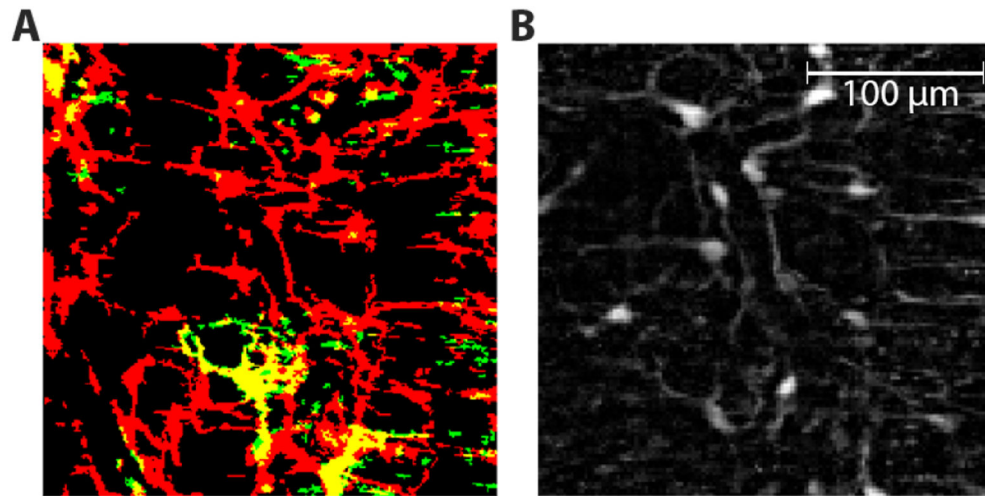


**Fig. 3:** Immunohistochemical stained ICC network and Ca<sup>2+</sup> frames were processed. a) Overlay of thresholded Kit and Ano1 stained ICC. Red indicated regions of tissue marked by Kit only, green indicates regions marked by Ano1 only, and yellow indicates regions marked by both Kit and Ano1. b) Location of Ca<sup>2+</sup> transients – higher intensity indicates regions with more activities

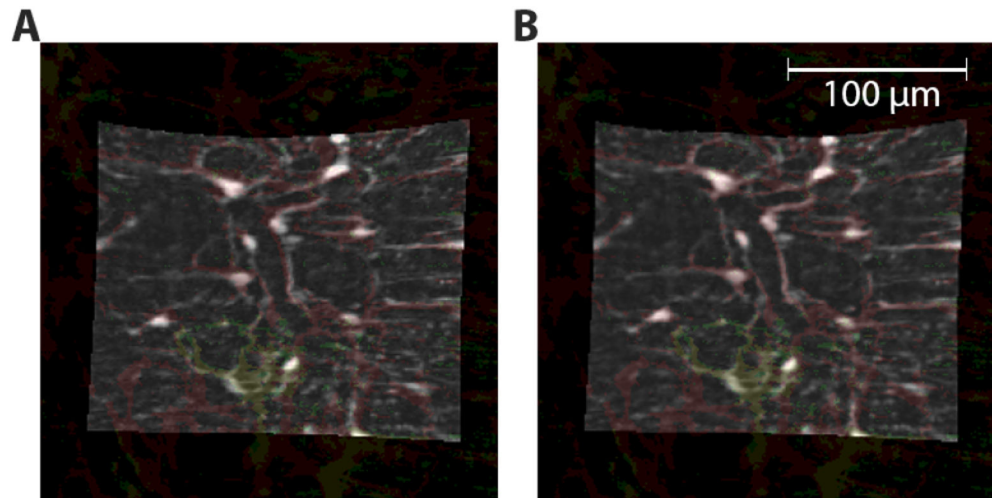


**Fig. 4:** Registration of Ca<sup>2+</sup> activity to structural data in two stages (a) Transformation of Ca<sup>2+</sup> transients according to the marked Ca<sup>2+</sup> recording FOV. Alignment of notable features in the Ca<sup>2+</sup> transients and structural data can be observed. (b) Ca<sup>2+</sup> transient data warped according to structural features to account for internal deformation resulting in better alignment of the two datasets.

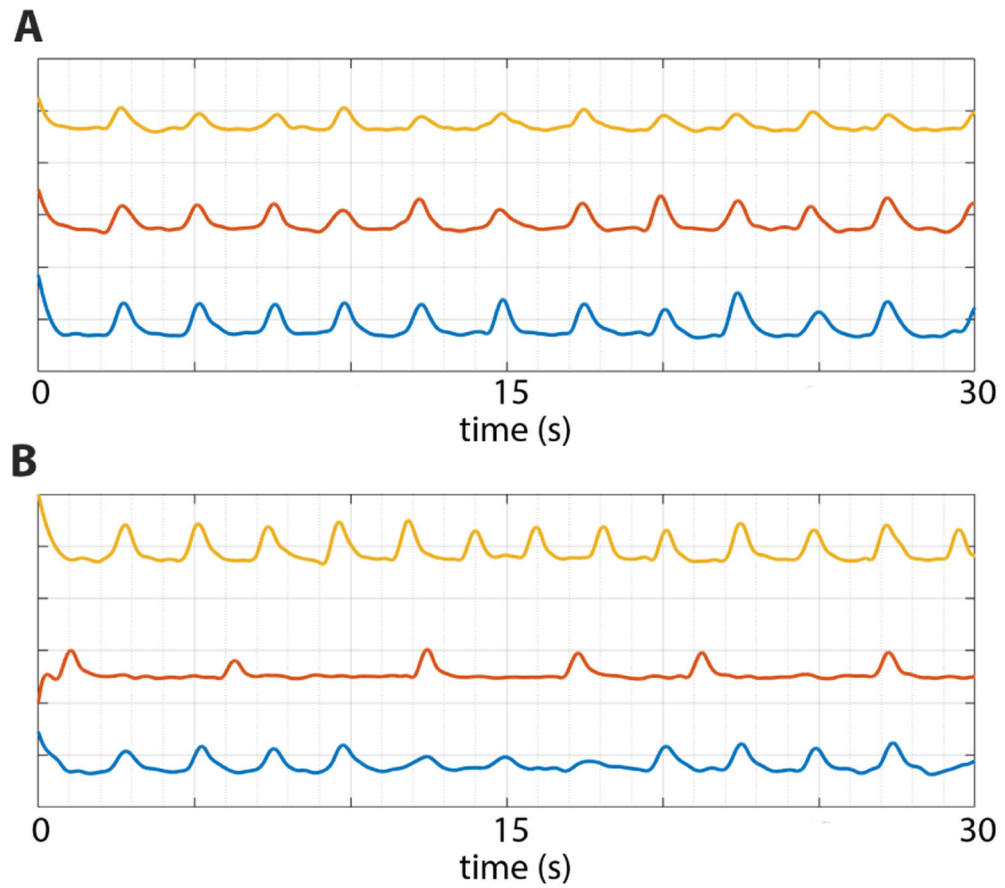


**Fig. 5:**  
A sample of normalized  $\text{Ca}^{2+}$  transient traces selected from (a)  $\text{Ano1}^+/\text{Kit}^+$  regions (b)  $\text{Ano1}^-/\text{Kit}^+$  regions. The traces were normalized to the maximum and minimum intensities in the entire  $\text{Ca}^{2+}$  transients FOV.